Ana C. N. Carloni<sup>1</sup> & João Luiz F. Azevedo<sup>2</sup>

<sup>1</sup>Instituto Tecnológico de Aeronáutica, 12228-900, São José dos Campos, SP, Brazil <sup>2</sup>Instituto de Aeronáutica e Espaço, 12228-904, São José dos Campos, SP, Brazil

#### **Abstract**

This paper explores the application of reduced-order models (ROMs) derived from unsteady Computational Fluid Dynamics (CFD) data for representing unsteady aerodynamics in aeroelastic stability analyses. Focusing on a NACA 0012 airfoil-based typical section, aerodynamic responses are computed using a 2-D Euler equation-based CFD solver. The study investigates three distinct ROM methodologies, namely Rational-Function Approximation (RFA), Eigensystem Realization Algorithm (ERA), and Dynamic Mode Decomposition (DMD). These ROMs are evaluated against established benchmark data, Single-Input/Multiple-Output (SIMO) simulations, and direct integration results. Notably, the ERA method overestimates the flutter speed by 5.0% in comparison to numerical benchmark results, while the DMD method underestimates it by 0.6%. Despite these variations, the reliance of the ERA model on a single unsteady CFD run showcases its practical utility. Conversely, the DMD method offers enhanced accuracy although requiring additional unsteady CFD runs for spline interpolation in this case. This investigation underscores the potential of ROMs in reducing computational expenses while effectively capturing critical aeroelastic phenomena.

Keywords: Aeroelastic analysis, Data-driven modeling, Transonic unsteady flow, Stability analysis

# 1 Introduction

Nonlinear aeroelasticity has been the focus of great interest in recent years as modern aircraft designs are evolving towards including increasingly lightweight and slender wings. These aspects directly impact the structural flexibility, ultimately favoring the occurrence of aeroelastic phenomena. While there are several tools currently available and recognized for certification in the subsonic regime, flutter prediction in transonic conditions still pose great challenges due to nonlinear behavior. In general, nonlinearities can be encountered in both structural and aerodynamic frameworks. Structural distributed nonlinearities typically originate from large structural displacements, while aerodynamic nonlinearities can originate from separated flow caused by large angles of attack and shock waves [1].

Conventional linear analysis methods are inadequate for addressing both structural and aero-dynamic nonlinearities. Although some extensions can partially relax linear assumptions in specific cases, a thorough modeling of nonlinear phenomena demands new approaches. Aerodynamic nonlinearities, especially those involving the processes of shock wave formation and dissipation, can only be accurately captured using high-fidelity computational fluid dynamics (CFD) simulations. Therefore, such numerical simulations are essential for effectively predicting flutter in the transonic regime [2]. The current standard procedure for aeroelastic analyses involves directly coupling the structural and aerodynamic models, resulting in an iterative process. This process involves calculating the instantaneous aerodynamic forces induced by a given structural deflection, and subsequently adjusting the structural deflection based on these newly computed aerodynamic loads. However, the computational cost of these high-fidelity simulations is often prohibitively high, thereby preventing their use in routine applications especially for complex systems.

Efficient analysis of transonic flows requires surrogate models to accurately represent unsteady aerodynamics at a fraction of the computational cost of high-fidelity CFD simulations. In this case, a reduced-order model (ROM) is a mathematical approximation capturing the prevailing dynamics of aerodynamic forces on structures in motion, such as aircraft wings experiencing gusts or vibrations. Reduced-order models aim to represent the complex aerodynamic behavior in a computationally efficient manner, enabling rapid analysis of aeroelastic phenomena while retaining sufficient accuracy for engineering applications [3].

The development of reduced-order models for unsteady aerodynamics has been significantly influenced by seminal contributions. An extensive overview of fluid-structure interaction modeling is presented in Ref. [4], emphasizing collaborative efforts to advance ROM techniques in aeroelasticity. In a subsequent work, Ref. [5] introduces innovative methodologies aimed at minimizing the number of unsteady CFD simulations required for ROM identification, particularly through the simultaneous excitation approach. Finally, Ref. [6] explores various data-driven techniques for developing advanced ROMs applicable to aeroelasticity.

Within this context, the present work investigates reduced-order models identified from unsteady CFD data to represent unsteady aerodynamics in aeroelastic stability analyses. The accuracy of these ROMs is evaluated by comparing the predicted flutter onset points with established benchmark results. This comparative analysis aims to validate the effectiveness of the ROMs in capturing critical aeroelastic phenomena and ensure their reliability for practical engineering applications.

The remainder of this paper is organized as follows. In Sec. 3, the CFD solver applied to compute the unsteady generalized aerodynamic forces in response to modal motions is outlined, including a brief description on the mesh movement in unsteady calculations. Section 4 briefly describes the reduced-order modeling techniques investigated in this paper. This is followed in Sec. 5 by the results of employing such data-driven ROM techniques to compose aeroelastic stability analyses. The paper is concluded in Sec. 6 with an overview and outlook of the methods.

## 2 Aeroelastic Test Case

The aeroelastic test case considered throughout this work is a NACA 0012 airfoil-based typical section with two degrees of freedom, namely plunge and pitch. Figure 1 schematically displays the typical section configuration in which h denotes the vertical displacement, positive downwards, and  $\alpha$  is the pitch mode coordinate, positive in the nose-up direction. In addition, c is the chord length, b is the semi-chord length,  $a_{\alpha}$  is the distance from the elastic axis to the center of mass normalized by the semi-chord,  $a_{\alpha}$  is the distance from mid-chord to the elastic axis normalized by the semi-chord, and  $b_{\alpha}$  are the stiffness coefficients associated with plunge and pitch modes, respectively.

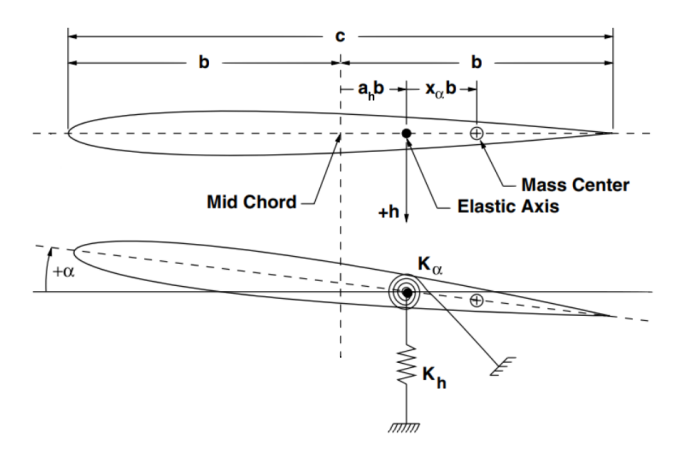


Figure 1 – Schematic representation of the typical section configuration, adapted from Ref. [7].

In the present study, the typical section is subjected to a transonic flow characterized by Mach number  $M_{\infty}=0.8$ , and has an initial angle of attack of  $\alpha_0=0$ . Following the work in Ref. [8], the aeroelastic system is defined through the parameters  $a_h=-2.0$ ,  $x_{\alpha}=1.8$ ,  $r_{\alpha}=1.865$ ,  $\mu=60$ ,  $\omega_h=\omega_{\alpha}=100$  rad/s, and  $\omega_r=\omega_{\alpha}$  is used as a reference frequency. In particular,  $r_{\alpha}$  is the airfoil dimensionless

radius of gyration about the elastic axis,  $\mu$  is the mass ratio, and  $\omega_h$  and  $\omega_\alpha$  are the uncoupled natural circular frequencies of the plunge and pitch modes, respectively. Note that the elastic axis is located upstream of the airfoil leading edge in order to simulate the dynamics of an outboard section of a sweptback wing [8, 9]. The same aeroelastic system is considered in Ref. [10] and, therefore, their numerical results are subsequently used for validation of the stability analyses results generated from each aerodynamic ROM.

In order to determine the governing equations, the aerodynamic effects in aeroelastic problems are usually represented exclusively through the resulting forces and moments acting on the structure as a forcing term. In this case, the equations of motion for a general aeroelastic system are written as

$$\mathbf{M}\ddot{\boldsymbol{\eta}}(\bar{t}) + \bar{\mathbf{K}}\boldsymbol{\eta}(\bar{t}) = \bar{\mathbf{Q}}_{\mathbf{a}}(\bar{t}) \tag{1}$$

where, for the typical section configuration, the generalized mass and stiffness matrices are, respectively,

$$\mathbf{M} = \begin{bmatrix} 1 & x_{\alpha} \\ x_{\alpha} & r_{\alpha}^{2} \end{bmatrix}, \quad \bar{\mathbf{K}} = \frac{1}{\omega_{r}^{2}} \begin{bmatrix} \omega_{h}^{2} & 0 \\ 0 & r_{\alpha}^{2} \omega_{\alpha}^{2} \end{bmatrix}, \tag{2}$$

and the generalized coordinate and generalized aerodynamic force vectors are given by

$$\boldsymbol{\eta}(\bar{t}) = \begin{cases} \frac{h(\bar{t})/b}{\alpha(\bar{t})} \end{cases}, \quad \bar{\mathbf{Q}}_{\mathbf{a}}(\bar{t}) = \frac{1}{\omega_r^2} \begin{cases} \frac{Q_{a_h}(\bar{t})}{mb} & \frac{Q_{a_\alpha}(\bar{t})}{mb^2} \end{cases}^{\mathsf{T}}. \tag{3}$$

This study focuses on efficiently determining the generalized aerodynamic force vector,  $\mathbf{\bar{Q}_a}$ , for arbitrary structural behavior,  $\boldsymbol{\eta}$ . By applying reduced-order modeling techniques derived from CFD data, we aim to develop a ROM that accurately represents unsteady aerodynamics in aeroelastic analyses.

# 3 Unsteady Aerodynamics

Initially, it is important to describe the CFD solver used to compute the generalized aerodynamic forces in response to prescribed modal motions during unsteady simulations. This explanation covers how the unsteady aerodynamic data sets, which are later used to derive the ROMs, are generated. The in-house CFD code [11, 12] employed in this study is based on the 2-D Euler equations. These equations describe two-dimensional, compressible, rotational, inviscid, and nonlinear flows, making the solver fully capable of capturing shock waves present in transonic flows. Initially, the equations are formulated in Cartesian coordinates to accommodate the use of unstructured meshes and the finite volume method. Following standard aerodynamic procedures, the equations are then reformulated in terms of algebraic vectors, including the conserved property vectors and flux vectors, with undisturbed flow quantities serving as the reference for nondimensionalization.

The algorithm employed is based on a cell-centered finite volume scheme where the stored information is the average of conserved properties across the control volume. Designed for unstructured triangular meshes, the flux is calculated as the sum of contributions from each edge, approximated from the average of neighboring conserved quantities as proposed in Ref. [13]. The dissipation operator is similar to those in Refs. [14, 15], but with modifications to adapt it for a cell-centered scheme. The numerical solution advances in time using a second-order accurate, 5-stage, explicit hybrid scheme derived from Runge-Kutta time-stepping [15]. In this scheme, the convective operator is evaluated at every stage of integration, while the artificial dissipation operator is evaluated only at the two initial stages.

For external flows, the CFD code begins with an undisturbed flow across the computational domain to establish steady-state calculations. In unsteady simulations, integration must be time-accurate, and the initial state must be physically correct. Therefore, before starting unsteady simulations, the CFD tool runs in steady-state mode to obtain a converged solution, which is then used as the starting point for unsteady calculations. Since unsteady calculations involve body motion, the computational mesh needs to be adjusted accordingly. This study employs a rigid mesh movement approach based on a prescribed pattern, with far-field boundary conditions accommodating this motion. All unsteady CFD simulations start from the converged steady-state solution and progress

through 100,000 time steps with a constant time step  $\Delta \bar{t}$  of 0.003 dimensionless time units. The same computational mesh used in Ref. [16] is applied to all test cases in this study. For further details on the CFD solver, the interested reader is referred to Refs. [11, 12, 17, 18].

# 4 Reduced-Order Modeling Techniques

Reduced-order models are crucial for encapsulating the essential dynamic mechanisms of aerodynamics, particularly considering the high number of degrees of freedom in discretized fluid dynamics equations [6]. In this section, we outline the reduced-order modeling techniques adopted in the present work in order to elucidate the modeling process of unsteady aerodynamics in transonic flows. For each approach, the initial data necessary for ROM identification comprise the prescribed modal motions of the airfoil in unsteady simulations, and the resultant aerodynamic coefficients.

# 4.1 Rational-Function Approximation

Significant attention has been directed in the past towards establishing methodologies that ensure consistency across analyses by translating digital CFD outputs into the continuous domain. One prominent technique for achieving this objective is the Rational-Function Approximation (RFA) method. Essentially, the RFA method involves approximating unsteady aerodynamic transfer functions within the Laplace domain using rational functions. This approximation serves as the foundation for constructing the stability matrix, thereby facilitating the resolution of the eigenvalue problem in stability analyses.

Although the model proposed in Ref. [19] is widely utilized for applications similar to those addressed in this study, the authors of Ref. [20] argue that their proposed model of aerodynamic state variables provides a more accurate representation of aerodynamic lags, which are identified as pivotal in understanding the flutter phenomenon. Reference [20] introduced rational-function approximations as second-order polynomials in the Laplace domain, augmented by an additional series of poles to introduce aerodynamic lags relative to structural modes. The determination of numerator coefficients is guided by a least-squares fit, while denominator coefficients, or poles, are treated as free parameters for optimization. The present study builds upon further investigations [16, 21] into two formulations proposed in Refs. [20, 22, 23], as presented in the following subsections.

# 4.1.1 First RFA Formulation

The rational function proposed in Ref. [23], which does not account for repeated or closely spaced poles, is initially selected. This choice is driven by the ease of constructing such RFAs for formulating aerodynamic state variables, as well as their extensive use in applications similar to those addressed in this study. In the Laplace domain, the rational-function approximation, here referred to as the first form, is expressed as

$$\boldsymbol{G}(\bar{s}) = \boldsymbol{A}_0 + \boldsymbol{A}_1 \frac{\bar{s}}{U^*} + \boldsymbol{A}_2 \left(\frac{\bar{s}}{U^*}\right)^2 + \sum_{n=1}^{n_{\beta}} \left(\boldsymbol{A}_{(n+2)} \frac{U^*}{\bar{s} + U^* \beta_n}\right), \tag{4}$$

In this context,  $U^*$  is the characteristic speed, and  $\beta_n$  represents poles introducing aerodynamic lags relative to structural modes, with  $n_\beta$  denoting the number of added poles and  $\mathbf{A}_n$  indicating the linear coefficient matrices used for approximation. The determination of RFA coefficients,  $\mathbf{A}_n$  and  $\beta_n$ , follows the methodology outlined in Refs. [22, 24]. In this approach, the lag parameters,  $\beta_n$ , undergo iterative evaluation using a simplex non-gradient optimizer [25], while the  $\mathbf{A}_n$  coefficients are derived through a least-squares fitting. Once the RFA coefficients are established, the aeroelastic system can be represented as a continuous-time state-space model. This involves integrating these coefficients into the stability matrix, as delineated in Ref. [21].

# 4.1.2 Second RFA Formulation

The second form of the RFA method is tailored to address situations where the optimized values of two or more poles are closely positioned, indicating the presence of repeated poles. This scenario occurs when the resulting approximate data matrix displays columns that are nearly identical,

rendering it nearly singular. Consequently, upon inversion of this matrix to compute the  $A_n$  coefficients associated with these lag parameters, they appear to be closely aligned in magnitude, yet divergent and of opposing signs. This phenomenon contributes to a poorly conditioned eigenvalue problem, wherein even minor variations in the elements of the matrices employed in the aerodynamic formulation, including numerical inaccuracies, can lead to significant fluctuations in the outcomes of aeroelastic stability analyses.

To address this challenge, Ref. [23] proposes a subtle adjustment to the lag terms in such scenarios. When two poles closely approach each other, they may be effectively consolidated into a single pole. However, this singular pole with double multiplicity must manifest in two terms of the polynomial, *i.e.*, one linear and one quadratic. This approach is extendable to instances featuring any arbitrary number of poles that occur very closely to each other. Despite originating from the phenomenon of repeated poles within the first RFA formulation, the rationale articulated in Ref. [23] reveals that the second form of the RFA can be applied even in those test cases where repeated poles do not occur in the first form of the approximation.

To accommodate poles with multiplicity, the second RFA formulation is expressed as

$$G(\bar{s}) = \mathbf{A}_{0} + \mathbf{A}_{1} \frac{\bar{s}}{U^{*}} + \mathbf{A}_{2} \left(\frac{\bar{s}}{U^{*}}\right)^{2} + \sum_{n=1}^{n_{\beta}} \left(\mathbf{A}_{(n+2)} \frac{U^{*}}{\bar{s} + U^{*} \beta_{n}}\right)$$

$$+ \sum_{n=n_{\beta_{1}}+1}^{n_{\beta}} \left(\mathbf{A}_{(n+n_{\beta}-n_{\beta_{1}}+2)} \frac{(U^{*})^{2}}{(\bar{s} + U^{*} \beta_{n})^{2}}\right)$$

$$+ \sum_{n=n_{\beta_{2}}+1}^{n_{\beta}} \left(\mathbf{A}_{(n+2n_{\beta}-n_{\beta_{1}}-n_{\beta_{2}}+2)} \frac{(U^{*})^{3}}{(\bar{s} + U^{*} \beta_{n})^{3}}\right) + \dots$$
(5)

Here,  $n_{\beta}$  denotes the total number of additional poles. It is assumed that  $\beta_1, \dots, \beta_{n_{\beta_1}}$  represent non-repeated poles, while  $\beta_{(n_{\beta_1}+1)}, \dots, \beta_{n_{\beta_2}}$  indicate poles occurring twice, and so on. Similar to the first RFA formulation, this formulation allows for a continuous-time state-space representation. This allows determining the stability matrix, which encapsulates the aerodynamic contribution within the aeroelastic system.

# 4.2 Eigensystem Realization Algorithm

Another technique discussed in the paper combines the Eigensystem Realization Algorithm (ERA) with the Observer Kalman Filter Identification (OKID) method. ERA builds simplified linear models by refining parameters using impulse response data [6, 26–28]. One advantage of the OKID/ERA approach is its adaptability for Multiple-Input/Multiple-Output (MIMO) systems, making it compatible with simultaneous excitation methods in unsteady CFD simulations. These algorithms facilitate the generation of discrete-time state-space models utilizing discrete-time impulse responses, known as Markov parameters, thereby offering a valuable tool for system identification procedures.

However, accurately measuring impulse responses in real-world scenarios can be challenging. In such cases, the OKID algorithm proves useful as it can estimate impulse responses using arbitrary input and output data pairs. Rather than directly presenting impulse responses obtained from dedicated experimental or simulated procedures, an alternative approach involves conducting initial experiments or simulations with arbitrary inputs. Subsequently, one can extract the impulse responses from the resulting input/output dataset using the OKID method. This approach offers the flexibility for users to select the most suitable input signals, thereby mitigating numerical and experimental issues. For instance, Ref. [29] demonstrates that CFD indicial responses are less sensitive to the choice of input amplitude and time step compared to CFD impulsive responses. Therefore, step-type inputs are considered the most convenient choice for computational simulations.

The Hankel matrix,  $\mathcal{H}$ , is constructed by arranging shifted time-series of impulse response mea-

surements,  $y_k = y(k\Delta t)$ , into a matrix

$$\mathcal{H} = \begin{bmatrix} y_1 & y_2 & \dots & y_{m_c} \\ y_2 & y_3 & \dots & y_{m_c+1} \\ \vdots & \vdots & \ddots & \vdots \\ y_{m_o} & y_{m_o+1} & \dots & y_{m_c+m_o-1} \end{bmatrix}.$$
 (6)

The singular value decomposition (SVD) of the Hankel matrix can, then, be computed

$$\mathcal{H} = \boldsymbol{U}\boldsymbol{\Sigma}\boldsymbol{V}^* = \begin{bmatrix} \tilde{\boldsymbol{U}} & \boldsymbol{U}_t \end{bmatrix} \begin{bmatrix} \tilde{\boldsymbol{\Sigma}} & \mathbf{0} \\ \mathbf{0} & \boldsymbol{\Sigma}_t \end{bmatrix} \begin{bmatrix} \tilde{\boldsymbol{V}}^* \\ \boldsymbol{V}_t^* \end{bmatrix} \approx \tilde{\boldsymbol{U}}\tilde{\boldsymbol{\Sigma}}\tilde{\boldsymbol{V}}^*, \tag{7}$$

allowing for the extraction of dominant characteristics in the time-series data. Only the initial r columns of matrices U and V, along with the principal  $r \times r$  block of the matrix  $\Sigma$ , are retained to derive a rank-r model. The remaining contribution from  $U_t\Sigma_tV_t^*$  is truncated.

Next, one can formulate a second, shifted Hankel matrix

$$\mathcal{H}' = \begin{bmatrix} y_2 & y_3 & \dots & y_{m_c+1} \\ y_3 & y_4 & \dots & y_{m_c+2} \\ \vdots & \vdots & \ddots & \vdots \\ y_{m_o+1} & y_{m_o+2} & \dots & y_{m_c+m_o} \end{bmatrix}$$
(8)

also based on measurements of impulse-response experiment or simulation. Finally, using matrices  $\mathscr{H}$  and  $\mathscr{H}'$ , the reduced-order model described in terms of a low-dimensional state,  $\tilde{x}$ , can be identified as

$$\tilde{\mathbf{x}}_{k+1} = \tilde{\mathbf{A}}\tilde{\mathbf{x}}_k + \tilde{\mathbf{B}}\mathbf{u} 
\mathbf{y} = \tilde{\mathbf{C}}\tilde{\mathbf{x}}_k,$$
(9)

where u denotes input signals and y denotes output signals, or measured data. Such ROM is defined based on the following matrices

$$\tilde{\mathbf{A}} = \tilde{\mathbf{\Sigma}}^{-1/2} \tilde{\mathbf{U}}^{\mathsf{T}} \mathcal{H}' \tilde{\mathbf{V}} \tilde{\mathbf{\Sigma}}^{-1/2},$$

$$\tilde{\mathbf{B}} = \tilde{\mathbf{\Sigma}}^{1/2} \tilde{\mathbf{V}}^{\mathsf{T}} \begin{bmatrix} \mathbf{I} & \mathbf{0} \\ \mathbf{0} & \mathbf{0} \end{bmatrix},$$

$$\tilde{\mathbf{C}} = \begin{bmatrix} \mathbf{I} & \mathbf{0} \\ \mathbf{0} & \mathbf{0} \end{bmatrix} \tilde{\mathbf{U}} \tilde{\mathbf{\Sigma}}^{1/2}.$$
(10)

For further details on the ERA and OKID algorithms, the reader is referred to Refs. [6, 30].

## 4.3 Dynamic Mode Decomposition

The dynamic mode decomposition (DMD) is a powerful data-driven method used to extract dynamic information from complex systems, capturing the prevailing modes that characterize the temporal evolution of the system. The primary goal of DMD is to decompose a sequence of snapshots from the system into modes, each associated with a specific frequency, and growth or decay rate. DMD is based on the idea of approximating the system evolution by a linear map that best fits the data, making it a versatile tool for analyzing both linear and nonlinear systems.

The DMD algorithm begins with collecting a series of snapshots of the system state for a given time interval. Let  $\mathbf{x}_1, \mathbf{x}_2, \dots, \mathbf{x}_m$  be these state snapshots. These snapshots are arranged into two matrices

$$\mathbf{X} = \begin{bmatrix} | & | & & | \\ \mathbf{x}_1 & \mathbf{x}_2 & \dots & \mathbf{x}_{m-1} \end{bmatrix} \quad \text{and} \quad \mathbf{X}' = \begin{bmatrix} | & | & & | \\ \mathbf{x}_2 & \mathbf{x}_3 & \dots & \mathbf{x}_m \end{bmatrix}$$
(11)

The core assumption in DMD is that there exists a linear operator A such that

$$\mathbf{x}_{k+1} \approx \mathbf{A}\mathbf{x}_k. \tag{12}$$

This implies

$$X' \approx AX$$
, (13)

establishing a linear relationship between the snapshots.

To find the best-fit linear operator A, DMD utilizes the SVD of the snapshot matrix X. Specifically,

$$X = U\Sigma V^*, \tag{14}$$

where U,  $\Sigma$ , and V are the matrices containing the left singular vectors, singular values, and right singular vectors, respectively. By projecting the dynamics onto the space spanned by the leading singular vectors, we form a reduced-order representation of A as

$$\tilde{\mathbf{A}} = \mathbf{U}^* \mathbf{X}' \mathbf{V} \mathbf{\Sigma}^{-1}. \tag{15}$$

This low-rank approximation captures the most significant features of the dynamics while discarding noise and less relevant information.

Finally, the eigenvalues and eigenvectors of  $\tilde{A}$  are computed to reveal the dynamic modes. The eigenvalue decomposition

$$\tilde{A}W = W\Lambda \tag{16}$$

provides the eigenvalues  $\Lambda$ , which indicate the growth or decay rates and oscillatory frequencies of the modes. The DMD modes are, then, reconstructed in the original high-dimensional space using

$$\mathbf{\Phi} = \mathbf{X}' \mathbf{V} \mathbf{\Sigma}^{-1} \mathbf{W}. \tag{17}$$

These modes, each evolving according to its corresponding eigenvalue, offer a clear and interpretable representation of the system dynamics. Thus, DMD decomposes the complex behavior into simpler components, facilitating understanding, prediction, and control of the system.

The approximate solution at all future times is given by

$$\mathbf{x}(t) \approx \sum_{k=1}^{r} \phi_k exp(\omega_k t) b_k = \mathbf{\Phi} exp(\mathbf{\Omega} t) \mathbf{b},$$
 (18)

where  $b_k$  is the initial amplitude of each mode,  $\Phi$  is the matrix whose columns are the DMD eigenvectors  $\phi_k$ , and  $\mathbf{\Omega} = diag(\boldsymbol{\omega})$  is a diagonal matrix whose entries are the eigenvalues  $\omega_k$ . The eigenvectors  $\phi_k$  are of the same size as the state,  $\boldsymbol{x}$ , and  $\boldsymbol{b}$  is a vector of the  $b_k$  coefficients. If the initial snapshot  $\boldsymbol{x}_1$  occurs at time  $t_1 = 0$ , then the initial conditions are given by

$$\boldsymbol{b} = \boldsymbol{\Phi}^{\dagger} \boldsymbol{x}_{1}, \tag{19}$$

such that  $\Phi^{\dagger}$  denotes the Moore-Penrose pseudoinverse of the matrix  $\Phi$ . The pseudoinverse is equivalent to finding the best-fit solution b in the least-squares sense. A thorough description of the DMD method can be found in Refs. [6, 31].

#### 5 Results

# 5.1 Aeroelastic Stability Analysis

To provide a comprehensive foundation for the evaluation of the proposed methodologies, two comparative datasets are introduced, namely the direct integration results and the Single-Input/Multiple-Output (SIMO) results. The direct integration approach involves the iterative solution of structural dynamic and unsteady aerodynamic equations. Conversely, the SIMO results are derived from a mode-by-mode analysis, where discrete step inputs prescribe each modal displacement of the typical section during unsteady CFD runs [5]. A notable limitation of the latter approach arises from the assumption that the transonic aeroelastic system behaves linearly with regard to modal displacements, once it is based on the convolution concept. Therefore, this study focuses exclusively on prescribed displacements with small amplitudes, where the linear assumption holds. Typical section displacements are constrained to 0.0001 degrees in pitch and 0.000001 chord lengths in plunge.

These datasets serve as benchmarks, enabling a robust comparison with the results obtained from the ROM formulations.

This section analyzes how the reduced-order modeling of the unsteady aerodynamics impacts the flutter onset within an aeroelastic framework. First, results from the RFA-based and DMD-based models are compared with numerical literature data extracted from Ref. [10], as well as with SIMO and direct integration results. The SIMO results are obtained with the first RFA formulation incorporating six optimized poles to approximate the aerodynamic transfer functions, followed by an eigenvalue analysis across dynamic pressure values. The direct integration results are determined by approximating time-domain CFD results through least-squares fitting with complex exponential functions, employing the technique presented in Ref. [32]. Moreover, the literature results are computed from Euler harmonic analyses, also approximating the resulting aeroelastic responses based on Ref. [32]. While acknowledging the susceptibility of literature data to numerical errors, we consider them valuable for facilitating meaningful comparisons within the context of the present study.

Figure 2 shows the eigenvalue-based root loci for varying dimensionless dynamic pressures. Amplified views on the first and second aeroelastic modes are presented in Figs. 2b and 2c. The characteristic dynamic pressure levels with resolution of 0.1 are distinguished using different colors. The first aeroelastic mode clearly exhibits flutter instability, with direct integration results closely resembling the benchmark literature results, as expected. However, significant differences are observed in the results obtained for the second aeroelastic mode, where direct integration results seem to follow a fairly distinct path in the s-plane when compared to the literature data. Such behavior can be explained by the greater impact of the first aeroelastic mode on the time response, as opposed to the second mode, a consequence of employing a curve fitting procedure that simultaneously determines damping and frequency characteristics for both aeroelastic modes within the direct integration solutions. Moreover, while SIMO results follow similar trends as the literature data, they do not exactly match such data.

The DMD-based ROM is formulated by including plunge and pitch displacements, along with their derivatives, to compose the system state. For each dynamic pressure value, a dynamical system described by Eq. 12 is identified using direct integration results as input snapshot data. The elements of the dynamic matrices, mapping temporal snapshots, are then interpolated using splines. With a consistent dynamic pressure resolution of 0.1, Fig. 2 shows that the eigenvalues from the DMD model closely align with those from direct integration, particularly for the first aeroelastic mode. However, for the second aeroelastic mode, while the DMD eigenvalues initially match the direct integration results at lower dynamic pressure levels, they begin to move away from those results as the dynamic pressure increases. This discrepancy, characterized by a decrease in frequency, leads the eigenvalues that more closely resemble the outcomes predicted by the SIMO approach.

The use of spline interpolation within DMD models offers a notable advantage of facilitating the computation of typical section time responses for intermediate dynamic pressure values, leading to a significant reduction in computational costs. This capability is a crucial aspect for accurately predicting the behavior of aeroelastic systems near the stability boundary. Moreover, by employing the DMD model to forecast the aeroelastic time response, the need for multiple additional unsteady CFD simulations, typically required by direct integration methods, is circumvented. Figure 3 displays the root locus derived from interpolated models, wherein the dynamic pressure resolution has been reduced to 0.001. However, to maintain clarity and avoid visual clutter, only a subset of the computed eigenvalues is shown. Aeroelastic stability analyses conducted using the intermediate models clearly indicate that flutter instability occurs between dimensionless dynamic pressure values of 0.49 and 0.50.

Both RFA formulations exhibit nearly identical root loci for the first and second aeroelastic modes, as indicated in Fig. 2. This reinforces the notion that the second RFA formulation does not notably enhance the fitting accuracy of the aerodynamic transfer functions, which establish the foundation for frequency-domain aeroelastic stability analyses. While these RFA methods closely align with SIMO results, discrepancies gradually emerge with rising dynamic pressure levels in the first aeroelastic mode. For completeness, Fig. 4 shows root loci in the complex z-plane using the ERA model with rank-6. The same dynamic pressure resolution of Fig. 2 is applied in this case. Figure 4b highlights

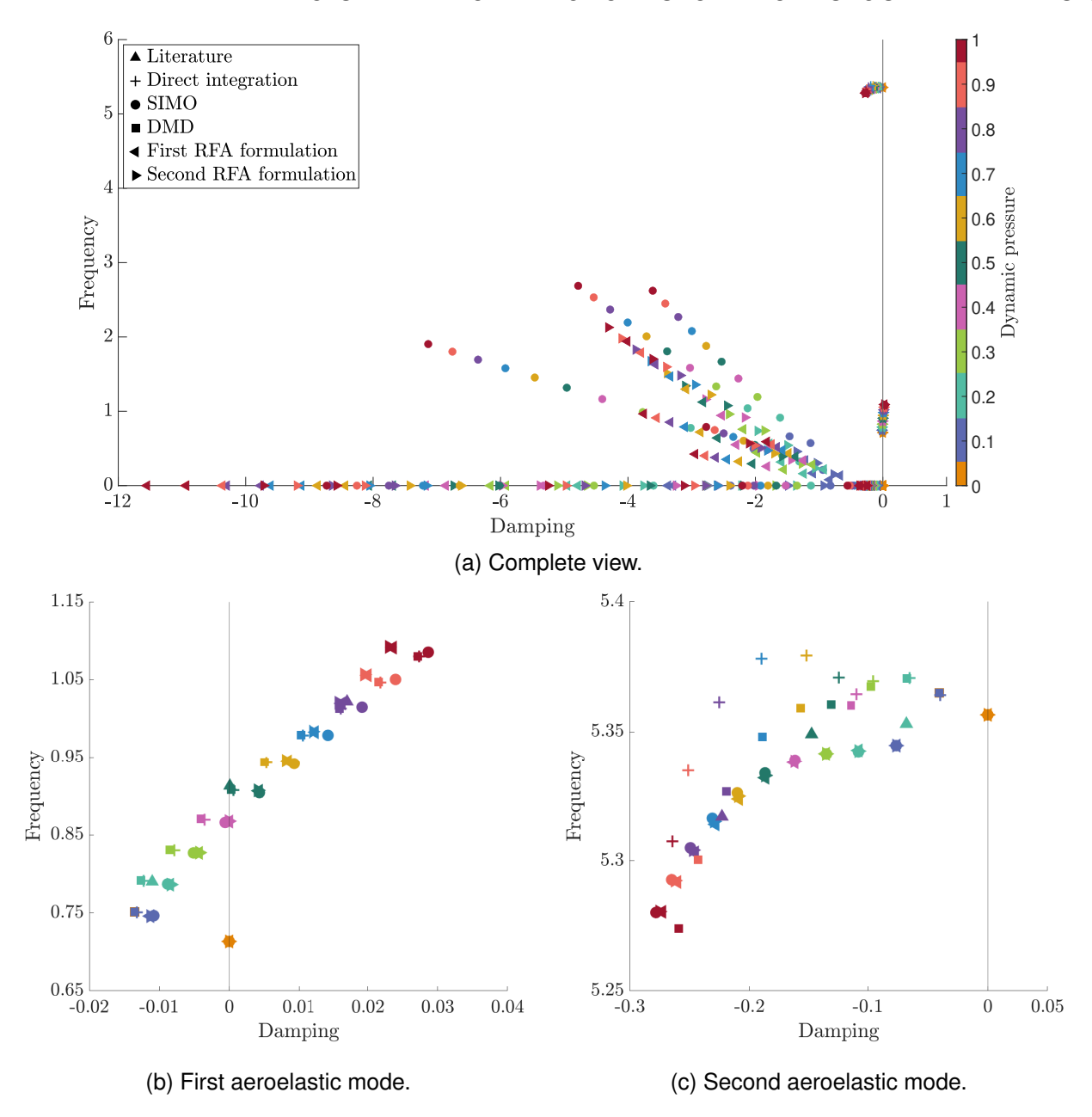


Figure 2 – S-plane root loci using several reduced-order modeling techniques.

the occurrence of flutter instability as the eigenvalues migrate beyond the unitary circle with increasing dynamic pressure levels.

# 5.2 Flutter Onset Identification

Table 1 compares the flutter onset parameters obtained in the present study with a reference numerical solution [10], showing the relative percentage difference labeled as  $\Delta$ . The benchmark inviscid results, shown as upward-pointing triangles in Fig. 2, are from a two-dimensional unsteady Euler code [14] extended to the aeroelastic analysis of airfoils. Besides the flutter onset parameters, *i.e.*, flutter speed or flutter dynamic pressure, the table also presents the aeroelastic frequencies and damping values at the flutter condition. In the inviscid dataset provided in Ref. [10], the modal damping of the first aeroelastic mode is reported simply as zero. As a result, the authors have preferred avoiding to calculate the relative error associated with this parameter. Flutter onset parameters include the flutter speed and flutter dynamic pressure, specifically denoting the characteristic speed and characteristic dynamic pressure at the onset of flutter. Except for the DMD model, all reduced-order models determine the flutter onset point by employing quadratic interpolation of the damping

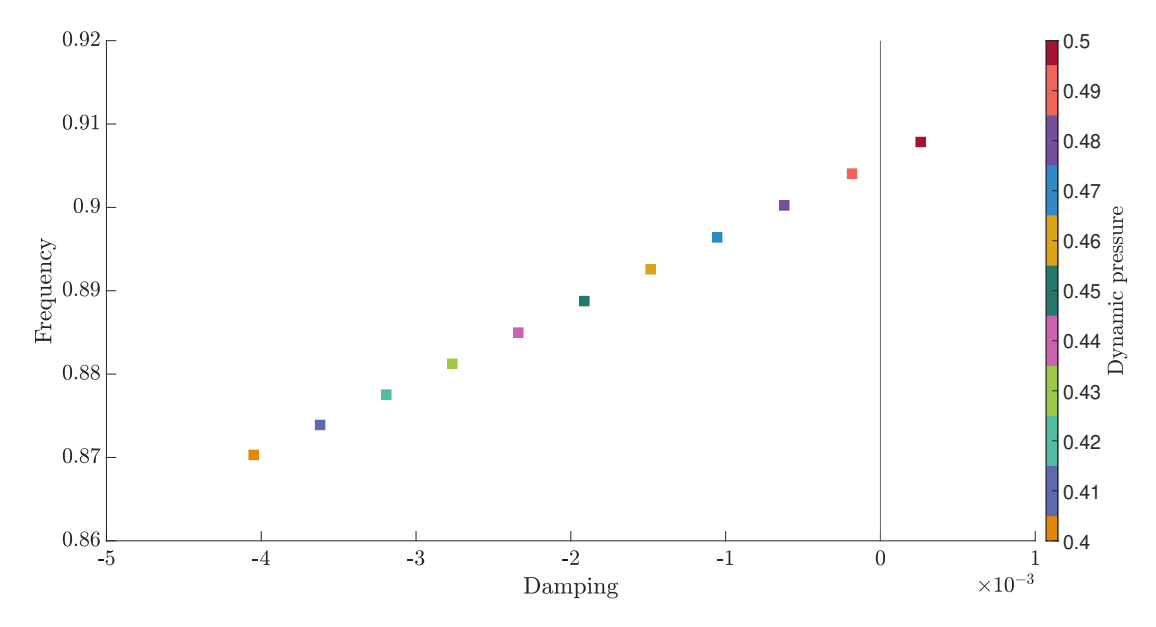


Figure 3 – S-plane root loci using DMD-based model in the proximity of flutter onset.

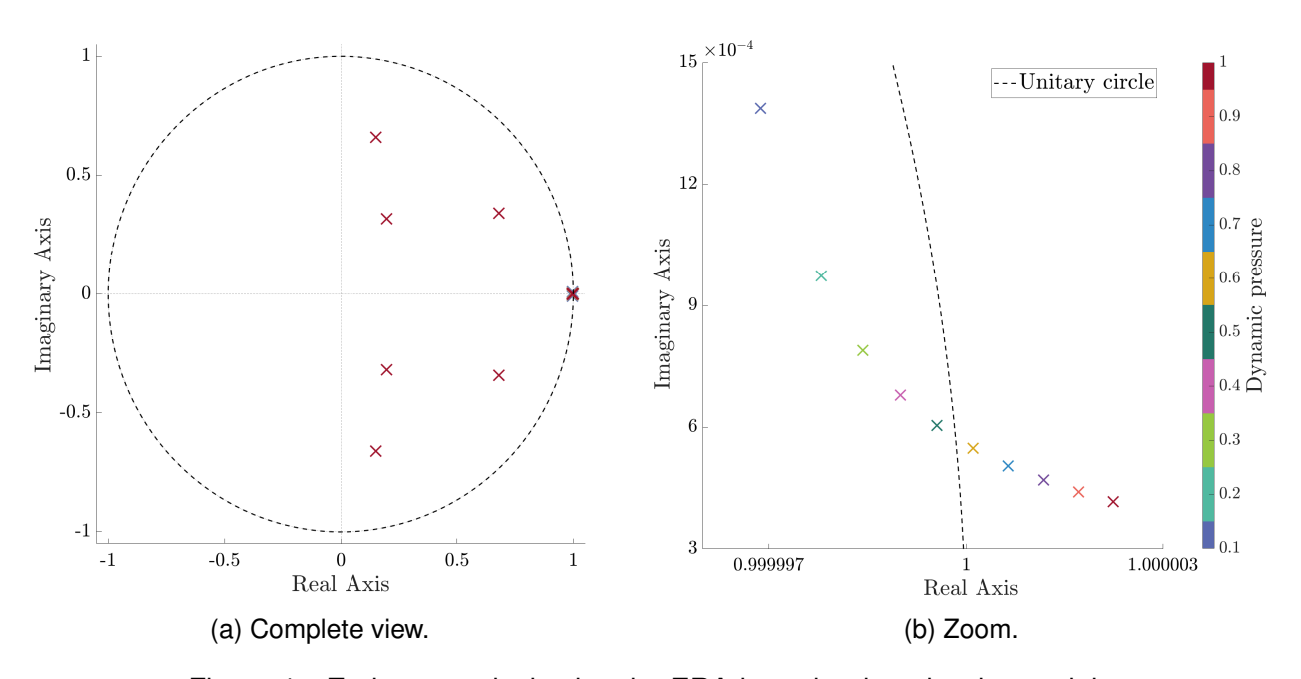


Figure 4 – Z-plane root loci using the ERA-based reduced-order model.

values nearest to the stability boundary. By employing this approach, consistent comparisons can be made with numerical benchmark results that also use quadratic interpolation.

The flutter onset speeds resulting from RFA formulations differ by 5.6% and 5.7% compared to the benchmark results. The second RFA formulation offers a slight improvement in estimating the flutter onset compared to the first RFA formulation. Moreover, there is a consistent underestimation of flutter onset parameters by the RFA results. This can be attributed to the limited range of pole positioning options, which compromises the accuracy of fitting discrete-time aerodynamic transfer functions based on CFD data. Despite the emergence of discrepancies between the results of RFA formulations and the reference SIMO approach in the first aeroelastic mode as dynamic pressure levels increase, as seen in Fig. 2b, the effect to the accuracy of flutter speed prediction resulting from this behavior is minimal. Actually, discrepancies between these calculations remain below 6%.

The ERA approach demonstrates a flutter speed overestimation of 5.0% compared to benchmark inviscid results, representing an improvement over the underestimation errors of 5.6% and 5.7% as-

Table 1 – Flutter onset results and comparison to literature data.

(8	a) First RFA formula	ation.	
Quantity	Ref. [10]	Current	$\Delta$ (%)
Damping (Mode 1)	0.000	$-5.11 \times 10^{-10}$	_
Frequency (Mode 1)	0.913	0.891	-2.5
Damping (Mode 2)	-0.148	-0.176	-19.2
Frequency (Mode 2)	5.349	5.334	-0.3
Flutter speed	5.48	5.17	-5.7
Flutter dynamic pressure	0.50	0.44	-11.0
(b)	Second RFA formu	ulation.	
Quantity	Ref. [10]	Current	$\Delta$ (%)
Damping (Mode 1)	0.000	$-1.39 \times 10^{-9}$	_
Frequency (Mode 1)	0.913	0.891	-2.4
Damping (Mode 2)	-0.148	-0.177	-19.4
Frequency (Mode 2)	5.349	5.334	-0.3
Flutter speed	5.48	5.17	-5.6
Flutter dynamic pressure	0.50	0.45	-10.8
	(c) ERA formulation	on.	
Quantity	Ref. [10]	Current	$\Delta$ (%)
Damping (Mode 1)	0.000	$-5.68 \times 10^{-14}$	_
Frequency (Mode 1)	0.913	0.925	1.3
Damping (Mode 2)	-0.148	-0.136	-8.3
Frequency (Mode 2)	5.349	4.556	-14.8
Flutter speed	5.48	5.75	5.0
Flutter dynamic pressure	0.50	0.55	10.3
	(d) DMD formulati	on.	
Quantity	Ref. [10]	Current	Δ (%)
Damping (Mode 1)	0.000	$3.7 \times 10^{-5}$	_
Frequency (Mode 1)	0.913	0.906	-0.8
Damping (Mode 2)	-0.148	-0.131	-11.7
Frequency (Mode 2)	5.349	5.360	-0.2
Flutter speed	5.48	5.45	-0.6
Flutter dynamic pressure	0.50	0.495	-1.0

sociated with the first and second RFA formulations, respectively. Furthermore, the ERA approach exhibits enhanced accuracy in capturing the damping and frequency values of the first aeroelastic mode, crucial for identifying flutter instability, when compared to RFA formulations. This improved capability is also evident in the DMD model, although more prominently. However, despite maintaining higher accuracy for the first mode, there is a significant decline in accuracy for the second mode frequency compared to RFA formulations. This aspect aligns with the capability of SVD-based models to capture the prevailing dynamics of the CFD response, which predominantly involves the first aeroelastic mode.

Finally, the flutter onset predictions from the DMD model are also outlined in Tab. 1. Employing the DMD model notably enhances the accuracy of assessing the damping and frequency parameters for the first aeroelastic mode, while also slightly improving the accuracy in predicting the frequency parameter for the second aeroelastic mode. In comparison to the benchmark result, the DMD model demonstrates outstanding accuracy, with 0.6% underestimation in predicting flutter speed and a 1.0% underestimation in flutter dynamic pressure. This notable enhancement surpasses all other ROMs,

which rely on RFA formulations and the ERA method.

In summary, predicting flutter onset in transonic flows depends significantly on how unsteady aerodynamics are modeled, with different approaches often leading to substantial variations. By integrating the simultaneous excitation approach into both RFA and ERA methodologies, aeroelastic analyses become more efficient, requiring only a single initial unsteady CFD run. This results in a notable reduction in computational expenses, mainly because fewer unsteady CFD runs are needed. However, the DMD model identified in this study relies on direct integration results, meaning that it requires conducting as many unsteady CFD runs as the number of initially evaluated dynamic pressures to gather the necessary data for the DMD method.

# **6 Concluding Remarks**

The paper investigates how reduced-order modeling techniques affect the identification of flutter onset in transonic aerodynamics, using a NACA 0012 airfoil-based typical section as a test case. The study relies on unsteady CFD data obtained by solving the Euler equations, primarily through a single unsteady CFD run alongside a previous steady CFD run. The low-order aerodynamic model is established using Rational-Function Approximations (RFAs), the Dynamic Mode Decomposition (DMD) method, and the Eigensystem Realization Algorithm (ERA).

The results demonstrate two notable techniques for identifying flutter onset boundaries: the ERA methodology, overestimating flutter speed by 5.0%, and the DMD formulation, underestimating it by 0.6%. Despite the ERA model showing a higher percentage error in flutter speed compared to the DMD model, it is emphasized here because it relies on a single unsteady CFD run. Conversely, while the DMD model presents a significantly lower percentage error in flutter speed, it would require at least two unsteady aeroelastic CFD runs if spline interpolation is employed to predict dynamic models for intermediate dynamic pressure levels. Such an additional computational cost might be acceptable, specially in light of the additional accuracy obtained in the estimation of the flutter onset condition. In any event, it is clear from the present study that ROM methodologies offer a promising solution for enhancing efficiency in aeroelastic analysis by reducing computational costs.

# 7 Acknowledgments

The authors acknowledge the financial support provided by the Fundação de Amparo à Pesquisa do Estado de São Paulo, FAPESP, under the Research Grants No. 2013/07375-0, 2021/11258-5, 2022/01397-0, and 2024/01647-2. The support from Fundação Coordenação de Aperfeiçoamento de Pessoal de Nível Superior, CAPES, under the Research Grants No. 88887.634461/2021-00 and 88887.609895/2021-00 is also acknowledged. The authors further acknowledge the support provided by Conselho Nacional de Desenvolvimento Científico e Tecnológico, CNPq, under the Research Grant No. 315411/2023-6.

#### 8 Contact Author Email Address

Ana C. N. Carloni: ana.nevescarloni@gmail.com. João Luiz F. Azevedo: joaoluiz.azevedo@gmail.com.

# 9 Copyright Statement

The authors confirm that they, and/or their company or organization, hold copyright on all of the original material included in this paper. The authors also confirm that they have obtained permission, from the copyright holder of any third party material included in this paper, to publish it as part of their paper. The authors confirm that they give permission, or have obtained permission from the copyright holder of this paper, for the publication and distribution of this paper as part of the ICAS proceedings or as individual off-prints from the proceedings.

## References

[1] Fonzi N, Brunton S L, and Fasel U. Data-Driven Modeling for Transonic Aeroelastic Analysis. *Journal of Aircraft*, Vol. 61, No. 2, pp 625-637, 2024.

- [2] Dowell E H and Hall K C. Modeling of Fluid-Structure Interaction. *Annual Review of Fluid Mechanics*, Vol. 33, pp 445-490, 2001.
- [3] Wang Q, Medeiros R R, Cesnik C E, Fidkowski K, Brezillon J, and Bleecke H M. Techniques for Improving Neural Network-Based Aerodynamics Reduced-Order Models. AIAA Scitech Forum 2019, San Diego, CA, AIAA Paper No. 2019-1849, pp 1-26, 2019.
- [4] Silva W A, Beran P S, Cesnik C E S, Guendel R E, Kurdila A, Prazenica R J, Librescu L, Marzocca P, and Raveh D E. Reduced-Order Modeling: Cooperative Research and Development at the NASA Langley Research Center. International Forum on Aeroelasticity and Structural Dynamics, Madrid, Spain, Paper IFASD 2001-008, pp 1-16, 2001.
- [5] Silva W A. Simultaneous Excitation of Multiple-Input/Multiple-Output CFD-Based Unsteady Aerodynamic Systems. *Journal of Aircraft*, Vol. 45, No. 4, pp 1267-1274, 2008.
- [6] Brunton S L and Kutz J N. *Data-Driven Science and Engineering: Machine Learning, Dynamical Systems, and Control.* Cambridge University Press, 2022.
- [7] Thomas J P and Dowell E H. Discrete Adjoint Approach for Nonlinear Unsteady Aeroelastic Design Optimization. *AIAA Journal*, Vol. 57, No. 10, pp 4368-4376, 2019.
- [8] Isogai K. On the Transonic-Dip Mechanism of Flutter of a Sweptback Wing. *AIAA Journal*, Vol. 17, No. 7, pp 793-795, 1979.
- [9] Alonso J and Jameson A. Fully-Implicit Time-Marching Aeroelastic Solutions. 32nd AIAA Aerospace Sciences Meeting and Exhibit, Reno, NV, AIAA Paper No. 94-0056, pp 1-11, 1994.
- [10] Rausch R D, Batina J T, and Yang H T Y. Euler Flutter Analysis of Airfoils Using Unstructured Dynamic Meshes. *Journal of Aircraft*, Vol. 27, No. 5, pp 436-443, 1990.
- [11] Marques A N and Azevedo J L F. Application of CFD-Based Unsteady Forces for Efficient Aeroelastic Stability Analyses. *Journal of Aircraft*, Vol. 44, No. 5, pp 1499-1512, 2007.
- [12] Marques A N and Azevedo J L F. Numerical Calculation of Impulsive and Indicial Aerodynamic Responses Using Computational Aerodynamics Techniques. *Journal of Aircraft*, Vol. 45, No. 4, pp 1112-1135, 2008.
- [13] Jameson A and Mavriplis D. Finite Volume Solution of the Two-Dimensional Euler Equations on a Regular Triangular Mesh. *AIAA Journal*, Vol. 24, No. 4, pp 611-618, 1986.
- [14] Batina J T. Unsteady Euler Airfoil Solutions Using Unstructured Dynamic Meshes. *AIAA Journal*, Vol. 28, No. 8, pp 1381-1388, 1990.
- [15] Mavriplis D J. Accurate Multigrid Solution of the Euler Equations on Unstructured and Adaptive Meshes. *AIAA Journal*, Vol. 28, No. 2, pp 213-221, 1990.
- [16] Azevedo J H A, Azevedo J L F, and Silva R G A. Effects of the Aerodynamic Data in a MIMO System Identification Framework for Aeroelastic Analyses. 54th AIAA/ASME/ASCE/AHS/ASC Structures, Structural Dynamics, and Materials Conference, Boston, MA, AIAA Paper No. 2013-1486, pp 1-37, 2013.
- [17] Marques A N. A Unified Discrete-Time Approach to the State Space Representation of Aeroelastic Systems. Master's thesis, Instituto Tecnológico de Aeronáutica, São José dos Campos, SP, Brazil, 2007.
- [18] Azevedo J H A. Aeroelastic Studies Using System Identification Techniques. Master's thesis, Instituto Tecnológico de Aeronáutica, São José dos Campos, SP, Brazil, 2013.
- [19] Roger K L. Airplane Math Modeling Methods for Active Control Design. AGARD CP–228, AGARD, 1977.

- [20] Eversman W and Tewari A. Modified Exponential Series Approximation for the Theodorsen Function. *Journal of Aircraft*, Vol. 28, No. 9, pp 553-557, 1991.
- [21] Marques A N and Azevedo J L F. A z-Transform Discrete-Time State-Space Formulation for Aeroelastic Stability Analysis. *Journal of Aircraft*, Vol. 45, No. 5, pp 1564-1578, 2008.
- [22] Eversman W and Tewari A. A Reduced Cost Rational-Function Approximation for Unsteady Aerodynamics. 31st AIAA/ASME/ASCE/AHS/ASC Structures, Structural Dynamics and Materials Conference, AIAA Paper No. 90-1155, pp 1418-1425, 1990.
- [23] Eversman W and Tewari A. Consistent Rational-Function Approximation for Unsteady Aerodynamics. *Journal of Aircraft*, Vol. 28, No. 9, pp 545-552, 1991.
- [24] Carloni A C N. Aeroelastic Analysis of Transonic Flutter with CFD-Based Reduced-Order Models. Master's thesis, Instituto Tecnológico de Aeronáutica, São José dos Campos, SP, Brazil, 2023.
- [25] Nelder J A and Mead R. A Simplex Method for Function Minimization. *The Computer Journal*, Vol. 7, No. 4, pp 308-313, 1965.
- [26] Raveh D E, Iovnovich M, and Nahom T. Wind-Tunnel Study of the ARMA Flutter Prediction Method. 59th AIAA/ASCE/AHS/ASC Structures, Structural Dynamics, and Materials Conference, AIAA SciTech Forum 2018, Kissimmee, FL, AIAA Paper No. 2018-0702, pp 1-24, 2018.
- [27] Silva W A, Chwalowski P, and Perry B. Evaluation of Linear, Inviscid, Viscous, and Reduced-Order Modelling Aeroelastic Solutions of the AGARD 445.6 Wing Using Root Locus Analysis. *International Journal of Computational Fluid Dynamics*, Vol. 28, No. 3-4, pp 122-139, 2014.
- [28] Silva W A. AEROM: NASA's Unsteady Aerodynamic and Aeroelastic Reduced-Order Modeling Software. *Aerospace*, Vol. 5, No. 2, p 41, 2018.
- [29] Raveh D E and Mavris D N. Reduced-Order Models Based on CFD Impulse and Step Responses. 42nd AIAA/ASME/ASCE/AHS/ASC Structures, Structural Dynamics, and Materials Conference and Exhibit, Seattle, WA, AIAA Paper No. 2001-1527, pp 1-19, 2001.
- [30] Juang J and Pappa R S. An Eigensystem Realization Algorithm for Modal Parameter Identification and Model Reduction. *Journal of Guidance, Control, and Dynamics*, Vol. 8, No. 5, pp 620-627, 1985.
- [31] Kutz J N, Brunton S L, Brunton B W, and Proctor J L. *Dynamic Mode Decomposition*. Society for Industrial and Applied Mathematics, 2016.
- [32] Bennett R M and Desmarais R N. Curve Fitting of Aeroelastic Transient Response Data with Exponential Functions. Technical Report NASA-77N21024, NASA Langley Research Center, Hampton, VA, 1976.